First-principles modeling of electron transport



2008 J. Phys.: Condens. Matter 20 064216

(http://iopscience.iop.org/0953-8984/20/6/064216)

IOP PUBLISHING JOURNAL OF PHYSICS: CONDENSED MATTER

J. Phys.: Condens. Matter **20** (2008) 064216 (7pp) doi:10.1088/0953-8984/20/6/064216

# First-principles modeling of electron transport

**K Stokbro**

Department of Computer Science, University of Copenhagen, Universitetsparken 1, DK-2100 Copenhagen, Denmark

E-mail: kurt.stokbro@gmail.com

Received 4 September 2007, in final form 10 October 2007
Published 24 January 2008
Online at stacks.iop.org/JPhysCM/20/064216

**Abstract**

The dimensions of electronic devices are rapidly decreasing and there is a need for a new generation of modeling tools that can accurately calculate the electrical properties of devices where atomic scale details and quantum effects are important. A promising framework for such calculations is density functional theory within the non-equilibrium Green's function formalism (NEGF-DFT). In this paper we present the basic framework and applications of the formalism. The applications include the calculation of the $I$–$V$ characteristics of a single molecule connected with gold electrodes and the spin-dependent electron transport through a magneto-tunnel junction consisting of MgO layers sandwiched between Fe electrodes.

For the formalism to be applied in semiconductor device modeling it needs to be able to handle many thousands of atoms. We discuss new developments and future aspects of the method important for semiconductor device modeling; in particular we show that for important classes of systems the approach scales linearly with the system size.

(Some figures in this article are in colour only in the electronic version)

## 1. Introduction: the need for quantum modeling in the electronics industry

The continuing downscaling of electronics devices poses new challenges to the semiconductor industry for each new device generation. At the nanometer length scale there are important quantum effects and the materials which were working well in previous device generations do not perform properly at the nanoscale and new materials need to be introduced. Eventually, not only the materials but also the basic device operation principles and geometries need to be revised.

The transition from the microscale to the nanoscale is challenging the semiconductor device modeling tools and a new generation of modeling tools which incorporate quantum effects and describe the atomic scale detail of the device must be introduced. The need for new modeling tools is detailed in the modeling section of the International Roadmap for the semiconductor industry [1].

In this paper we focus on new tools for atomic scale modeling of the electrical properties of emerging electronic devices. Such devices may consist of completely new materials like molecules, carbon nanotubes, nanowires or use new quantities like the electron spin to process information. These materials have complex electronic properties that depend on the detailed device geometry and an accurate quantum chemical model of the atomic scale geometry is needed. We will describe the use of non-equilibrium Green's functions (NEGF) combined with electronic structure methods to model the electrical properties of nanoscale devices [2–11]. The electronic structure model is constructed from first principles using density functional theory (DFT) within a localized basis set framework [12]. We will only discuss the formalism for coherent transport, i.e. it is assumed that the electron only undergoes scattering events described by the DFT one-electron Hamiltonian; thus events not included are inelastic scattering by phonons or dynamical electron–electron interactions. There is work in progress to extend the method to include such effects [13].

We will present applications of the method for modeling the electrical properties of molecular electronics devices and spin-dependent electron transport in magneto-tunnel junctions. The examples are for systems with a few hundred atoms and the calculations have been performed on a single workstation. However, we will show that the underlying formalism for the NEGF-DFT calculations has O($N$) scaling and with new proper parallel algorithms and the use of supercomputers it is a promising approach for studying complete devices with many thousand atoms.

 

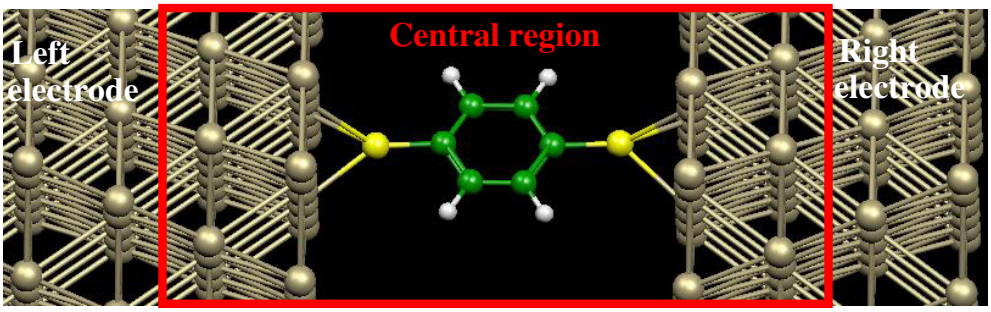


**Figure 1.** Illustration of the geometry of a two-probe system. The system consists of a central region in contact with two electrodes. The electrodes form a semi-infinite periodic lattice and it is assumed that the central region is sufficiently large that the electron density in the electrode region has retained its bulk value. The properties of the electrode region can then be obtained from a calculation of an electrode cell with periodic boundary conditions.

The division of the paper is the following. In section 2 we briefly introduce the NEGF-DFT approach and in section 3.1 we discuss simulations of electron transport through a single molecule, while section 3.2 is devoted to modeling spin-dependent transport through an Fe–MgO–Fe sandwich structure. In section 4 we discuss work in progress for extending the methodology to encompass full semiconductor devices, and in section 5 we conclude.

## 2. NEGF-DFT model of electron transport in nanoscale devices

An atomic scale description of an electronic device requires a detailed model of the interaction between the electrons and the individual atoms. At the atomic scale such a description must be based on a quantum mechanical model. The most fundamental description is through the Schrödinger equation involving all the electrons and the ionic cores of the atoms. The main numerical problem with the Schrödinger equation is that it couples the motion of the electrons and this makes a general solution intractable. A very popular strategy for avoiding solving the full Schrödinger equation is using a mean field (MF) model, where each electron is described as an independent particle interacting with the MF from all the other electrons. This is usually calculated through the total electron density and since the electron density is determined from the electron wavefunctions the MF approach gives rise to a set of coupled equations that must be solved self-consistently.

One of the most successful MF approaches is density functional theory (DFT) invented by Kohn and co-workers more than 40 years ago [14, 15]. In DFT each electron is influenced by a MF determined from the total electron density through a classical electrostatic contribution, the so-called Hartree potential, and an additional term, the exchange–correlation potential, which arises from the quantum mechanical nature of the electrons. The exchange–correlation potential can only be calculated approximately, and there is a strong effort to develop new and improved exchange–correlation functionals. Popular choices are the local density approximation (LDA) [16] and generalized gradient approximation (GGA) [17] to DFT, and these approximations have proved very successful in describing the energetics of molecules and crystals. In this paper we use DFT to model electron transport properties and it will be important to have a good description of the electron energy levels. The LDA and GGA are known to underestimate energy gaps in insulating materials and results based on these approximations must therefore be analyzed with care in order to judge the validity of the results. Recent progress in the development of DFT functionals [18] seems promising for correcting this deficiency of the LDA and GGA.

The NEGF-DFT description of electron transport is based on the Kohn–Sham equations which introduce an equation of motion for each electron through the one-electron Schrödinger equation

$$\left[-\frac{\hbar^2\nabla^2}{2m} + V^{\text{eff}}(\mathbf{r})\right]\psi_\alpha(\mathbf{r}) = \varepsilon_\alpha\psi_\alpha(\mathbf{r}), \tag{1}$$

where $\psi_\alpha(\mathbf{r})$ is the wavefunction of the electron in orbital $\alpha$ and $V^{\text{eff}}(\mathbf{r})$ is the DFT mean field potential from the other electrons.

The DFT equations have mainly been solved for isolated systems like molecules where fixed boundary conditions can be applied or periodic systems like crystals where it is possible to use periodic boundary conditions. In this paper we will discuss device geometries where two crystalline materials are coupled together through a central region, as illustrated in figure 1. Such a system we call a two-probe system. To treat the two-probe system we divide it into three regions, left electrode, central region and right electrode. It is assumed that the electrode parts have bulk properties and for metallic electrodes this condition is easily met by including a few metallic layers in the central region. The first step in the two-probe technique is to calculate the properties of the electrodes using standard DFT techniques for periodic systems. The solution for the electrodes then sets up boundary conditions for the central region and the DFT equations for this region is then solved self-consistently.

In order to be able to decompose the one-electron Schrödinger equation, (1), into three regions, we expand the one-electron wavefunction in basis functions, $\phi_i(\mathbf{r})$, that are localized around each atom,

$$\psi_\alpha(\mathbf{r}) = \sum_i c_{\alpha i}\phi_i(\mathbf{r}), \tag{2}$$

where $c_{\alpha i}$ are the expansion coefficients. (1) can now be written as a matrix equation

$$\bar{H}\mathbf{c}_\alpha = \varepsilon_\alpha \bar{S}\mathbf{c}_\alpha, \tag{3}$$

where $\mathbf{c}^\alpha$ is a vector of the expansion coefficients for orbital $\alpha$ and the Hamiltonian $\bar{H}$ and overlap matrix $\bar{S}$ are defined through the integrals

$$H_{ij} = \int_V \phi_i(\mathbf{r})\left[-\frac{\hbar^2\nabla^2}{2m} + V^{\text{eff}}(\mathbf{r})\right]\phi_j(\mathbf{r})\,\mathrm{d}\mathbf{r}, \tag{4}$$

$$S_{ij} = \int_V \phi_i(\mathbf{r})\phi_j(\mathbf{r})\,\mathrm{d}\mathbf{r}. \tag{5}$$

The Hamiltonian and overlap matrices are block tridiagonal matrices, and can be separated into diagonal blocks, $H_{\text{LL}}$, $H_{\text{CC}}$, $H_{\text{RR}}$, and couplings $H_{\text{LC}}$, $H_{\text{RC}}$. As discussed above, the electrode region has periodic boundary conditions, and its properties are calculated by conventional DFT methods for periodic structures. To calculate the electron density of the central region we need to calculate the $G_{\text{CC}}$ part of the retarded Green's function, defined through matrix inversion,

$$G_{\text{CC}}(\varepsilon) = [(\varepsilon + \mathrm{i}\delta)\bar{S}_{\text{CC}} - \bar{H}_{\text{CC}} - \bar{\Sigma}^{\text{L}}_{\text{CC}} - \bar{\Sigma}^{\text{R}}_{\text{CC}}]^{-1}, \tag{6}$$

where $\delta$ is an infinitesimal and the self-energies, $\bar{\Sigma}^{\text{L}}_{\text{CC}}$, $\bar{\Sigma}^{\text{R}}_{\text{CC}}$, describe the coupling between the central region and the electrodes. Several efficient algorithms exist for calculating the self-energies from the self-consistent Hamiltonian of the electrodes [19, 20].

In the equilibrium situation where there is no applied bias the density matrix, $D_{ij}$, can be obtained from the retarded Green's function through

$$D_{ij} = \frac{1}{\pi}\int_{-\infty}^{\mu} \text{Im}[G_{ij}(\varepsilon)]\,\mathrm{d}\varepsilon, \tag{7}$$

where $\mu$ is the equilibrium chemical potential of the system. In the non-equilibrium situation where there is an applied bias, $V$, the chemical potentials in the left and right electrode are different, and related by $\mu_{\text{L}} - \mu_{\text{R}} = eV$. In this case it is necessary to use NEGF theory, and the equation for the density matrix takes the form

$$\bar{D} = \frac{1}{\pi}\int_{-\infty}^{\mu_{\text{L}}} \bar{G}(\varepsilon)\,\text{Im}[\bar{\Sigma}^{\text{L}}]\bar{G}(\varepsilon)^\dagger\,\mathrm{d}\varepsilon + \frac{1}{\pi}\int_{-\infty}^{\mu_{\text{R}}} \bar{G}(\varepsilon)\,\text{Im}[\bar{\Sigma}^{\text{R}}]\bar{G}(\varepsilon)^\dagger\,\mathrm{d}\varepsilon. \tag{8}$$

From the density matrix we can obtain the electron density through

$$n(\mathbf{r}) = \sum_{ij} D_{ij}\phi_i(\mathbf{r})\phi_j(\mathbf{r}). \tag{9}$$

The different steps in the algorithm are summarized in table 1 and we see that the calculation of the density closes the self-consistent loop.

With the self-consistent DFT solution we have an effective one-electron description of the system and we will calculate the electron transport properties by using the Kohn–Sham Hamiltonian for propagating each electron. The propagation is quantified by the transmission coefficient. $T_{\text{L}\to\text{R}}(\varepsilon)$, gives the total number of states propagating from left to right at a given energy. Due to time-reversal symmetry of the underlying quantum mechanical equations the transmission coefficient for states propagating from right to left will be similar, $T_{\text{R}\to\text{L}}(\varepsilon) = T_{\text{L}\to\text{R}}(\varepsilon)$, and we therefore drop the subscript and use $T(\varepsilon)$. In order to obtain the electrical current we need to weight $T(\varepsilon)$ with the electron occupation in the electrode reservoirs, $n_{\text{F}}(\varepsilon)$. We will assume that $n_{\text{F}}(\varepsilon)$ can be described by a Fermi distribution, and the total current is given by

$$I = \frac{e}{h}\int_{-\infty}^{\infty} T(\varepsilon)[n_{\text{F}}(\varepsilon - \mu_{\text{L}}) - n_{\text{F}}(\varepsilon - \mu_{\text{R}})]\,\mathrm{d}\varepsilon. \tag{10}$$

By linear expansion around $\mu = \mu_{\text{L}} = \mu_{\text{R}}$, it is easy to show that the conductance, $\sigma$, is given by

$$\sigma = \frac{e^2}{h}T(\mu). \tag{11}$$

**Table 1.** The table summarizes the steps involved in solving the self-consistent DFT Kohn–Sham equations for a two-probe system. For each step we summarize the input and output of the algorithm and its computational complexity when implemented using localized basis functions. The complexity is given in terms of the number of atoms $N$ and the area of the electrode cell $A$.

| Step | Algorithm | Complexity |
|---|---|---|
| 1 | $n(\mathbf{r}) \to V^{\text{eff}}(\mathbf{r})$ | $\text{O}(N \log N)$ |
| 2 | $V^{\text{eff}}(\mathbf{r}) \to \bar{H}$ | $\text{O}(N)$ |
| 3 | $\bar{H} \to \bar{G}$ | $\text{O}(N^3), \text{O}(NA^3)$ |
| 4 | $\bar{G} \to \bar{D}$ | $\text{O}(N)$ |
| 5 | $\bar{D} \to n(\mathbf{r})$ | $\text{O}(N)$ |

## 3. Applications

In the previous section we gave a brief overview of the NEGF formalism for calculating electron transport. There exist several independent implementations of the approach [2–11] with slight differences in technical implementations. In the following we will present the application of the formalism with two examples obtained with the TranSIESTA [2] and the related Atomistix Tool Kit (ATK) implementation, and further technical details of these implementations can be found in [2]. The first example shows the calculation of the $I$–$V$ characteristics of a molecule coupled with two metal electrodes [21]; in the second example we calculate the tunneling magnetoresistance (TMR) of different magneto-tunnel junctions [22].

### *3.1. Electrical properties of a Tour wire connected with Au(111) electrodes*

In this section we will present calculations of the electrical properties of a dithiol phenylene–ethynylene oligomer, popularly called a Tour wire, between two gold electrodes [21]. A schematic of the geometry is shown in figure 2(a), and the atomic details of the system are similar to figure 1 except that the phenyl ring is substituted with the phenylene–ethynylene oligomer. Figure 2(b) illustrates the electronic structure of the LL, CC and RR parts of the system, which gives rise to

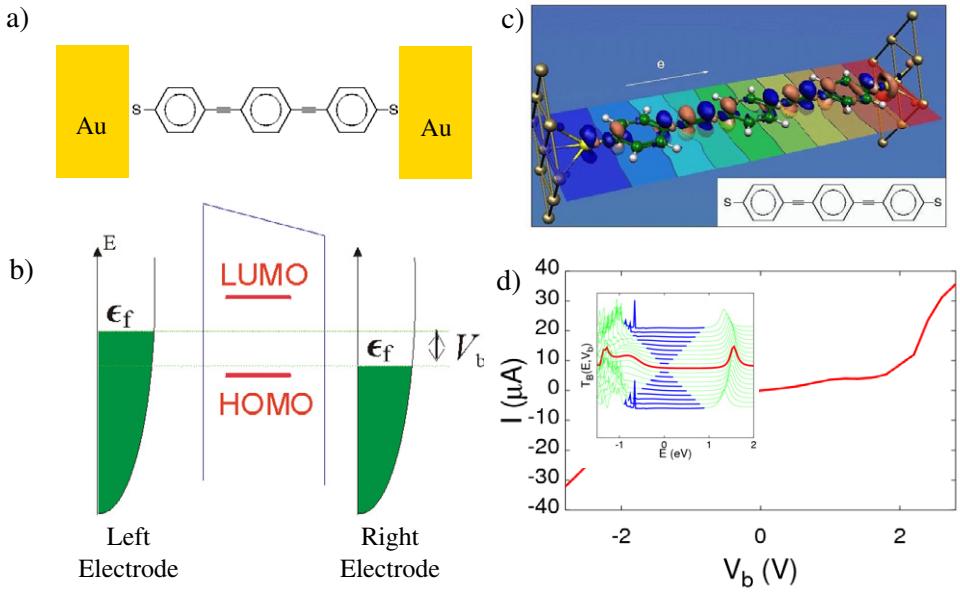


**Figure 2.** (a) Schematic of a Tour wire connected with two gold electrodes. (b) Illustration of the electronic structure of the system. (c) The contour line shows the voltage drop between the gold surfaces for an applied bias of 1 V and the iso-surface shows the induced density due to the applied bias. (d) Calculated current–voltage characteristics. The inset shows the transmission coefficient as a function of the electron energy, and each curve corresponds to different applied biases. The dark central part (blue online) of the curves shows the energy range within the bias window.

metallic bands in the electrodes and discrete levels within the molecule. The key quantity to be calculated is $T(\varepsilon)$, and it gives the fraction of electrons transmitted from left to right through the central region. $T(\varepsilon)$ is related to the number of propagating waves in the electrode and the available number of transmission channels in the central region. The inset in figure 2(d) shows $T(\varepsilon)$ as a function of the electron energy for different applied biases. The dark central part (blue online) of each curve shows the bias window, i.e. the energy region between the left and right chemical potentials. The bold (red online) middle curve corresponds to the equilibrium case where there is no applied bias. For each curve we define the zero energy as the average chemical potential of the two electrodes. There are two main peaks, one peak above the zero energy and one below. The position of the peak at positive energy is correlated with the energy of the lowest unoccupied molecular orbital (LUMO) of the Tour wire, and the position of the peak at negative energy is correlated with the energy of the highest occupied molecular orbital (HOMO). Thus, these peaks correspond to easy transmission of electrons from left to right, since at these energies an electron can use the molecular orbitals of the Tour wire to propagate through the device. We also note that the different curves are rather similar and the external bias therefore only has a small effect on the scattering properties of the device.

From $T(\varepsilon)$ it is easy to calculate the electrical current using (10). Note that only energies within the bias window contribute to the integral. The curve in figure 2(d) shows the calculated $I$–$V$ characteristics. The curve has a linear slope and an onset around 2 V. From inspections of $T(\varepsilon)$ we see that the onset is related to the HOMO entering the bias window. Thus, the current is related to transmission through the HOMO and we may conclude that the molecule behaves as a hole conductor when contacted with gold electrodes. The zero bias conductance of the molecule is 2.0 $\mu$S, similar to calculated values for a closely related molecule (OPV3) [23], and in excellent agreement with the recent experimental result of a conductance of 1.5 $\mu$S for OPV3 [24].

The contour plot in figure 2(c) shows the voltage drop through the system for an applied bias of 1 V. It can be seen that the voltage drop is nearly linear, and the molecular response to the applied bias is similar to that of a dielectric material [21]. The dielectric constant of the phenyl rings is slightly higher than that of the ethynylene bonds, and we see that the contour line spacing is larger and the electric field thereby smaller inside the phenyl rings compared to the rest of the molecule.

### *3.2. Spin-dependent transport in magneto-tunnel junctions*

In our next example we will investigate the spin-dependent transport in magneto-tunnel junctions (MTJ). A MTJ consists of an insulator sandwiched between two magnetic materials, and we will calculate how its resistance depends on the relative magnetization directions of the two electrodes. The figure of merit is the tunnel magnetoresistance

$$\mathrm{TMR} = \frac{\sigma_{\uparrow\uparrow} - \sigma_{\uparrow\downarrow}}{\sigma_{\uparrow\downarrow}}, \tag{12}$$

where $\sigma_{\uparrow\uparrow}$ is the conductance per unit area when the electrodes are magnetized in the same direction, and $\sigma_{\uparrow\downarrow}$ is the conductance when they are oppositely magnetized.

In 2001 it was predicted by Butler *et al* that MgO layers between Fe electrodes could display TMR values higher than 1000% [25]; more than one order of magnitude higher than

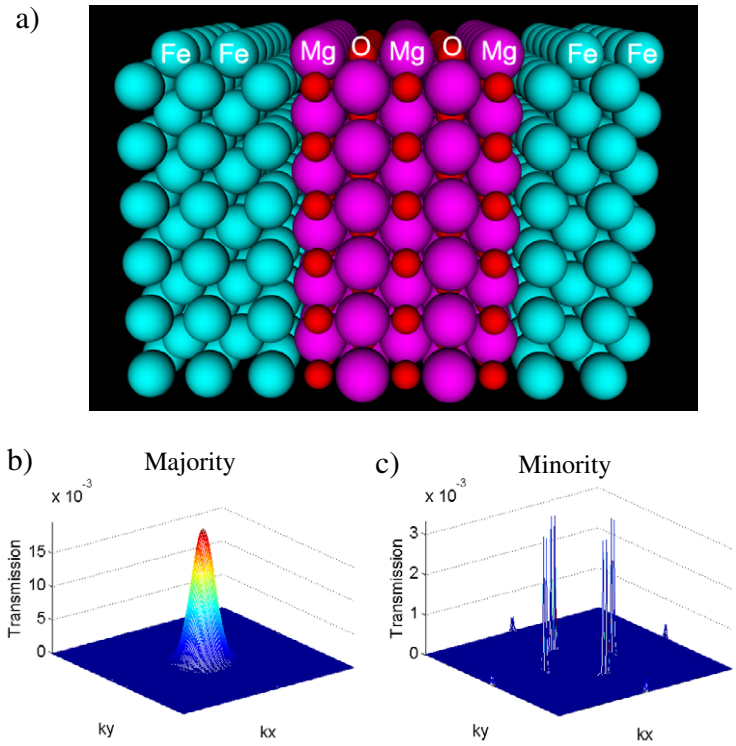


**Figure 3.** (a) The atomic geometry of the Fe–MgO–Fe system with five MgO layers. (b) Transmission coefficient of majority electrons at the Fermi energy as a function of the parallel momentum; (c) a similar plot but for minority electrons.

for $AlO_2$ based devices which were popular at that time. After refining the deposition process, experimentalists found in 2004 that MgO based MTJs show TMR in excess of 180% [26] and this has sparked a large focus on MgO based materials for spintronics applications. In the following we present calculational studies of the TMR of MgO based MTJs and the effect of different interface layers on the TMR [22].

Figure 3(a) shows the geometry of five MgO layers sandwiched between two Fe electrodes. The structure is described using a periodic $(1 \times 1)$ cell in the directions parallel with the interface (denoted $x$, $y$ directions). In the perpendicular direction, the $z$ direction, the system is divided into a central region containing the five MgO layers surrounded by three Fe layers to each side, and a left and right electrode region with three Fe layers each [22]. The periodic boundary conditions in the $x$, $y$ directions conserve the parallel momentum of the electron and the transmission coefficient, $T(\varepsilon, \mathbf{k}_\parallel, \sigma)$, depends on three quantum numbers, energy, $\varepsilon$, parallel momentum, $\mathbf{k}_\parallel$, and electron spin, $\sigma$.

Figures 3(b) and (c) show $T(\varepsilon, \mathbf{k}_\parallel, \sigma)$ for electrons at the Fermi energy, $\varepsilon = \varepsilon_F$, and with parallel magnetization of the electrodes. Figure 3(b) shows the result for the majority electrons, and it shows a strong dependence on the electron parallel momentum, $k_x, k_y$. The plot has a bell shaped form with maximum at $\mathbf{k}_\parallel = 0$. This shape can be understood from a WKB theory of transmission through a barrier

$$T(\varepsilon, \mathbf{k}_\parallel) \propto \exp\left(-\sqrt{\frac{2m_0}{\hbar^2}(\varepsilon - \varepsilon_v) + k_\parallel^2}\right), \qquad (13)$$

where $m_0$ is the effective mass and $\varepsilon_v$ is the valence band edge of the insulator. This equation describes that the energy difference $\varepsilon - \varepsilon_v$ sets up an effective barrier for the electron tunneling through the insulator.

For the minority electrons the situation is very different, as illustrated in figure 3(c). In this case there is no single peak in the transmission spectrum and the overall transmission is an order of magnitude smaller than for the majority electrons. The different behavior can be understood from the different band structure of the minority electrons compared to the majority electrons. At $\mathbf{k}_\parallel = 0$ the majority electrons have s-like character and this symmetry is only weakly damped when propagating through the MgO insulator. The minority bands have d-like symmetry and this symmetry is strongly damped when propagating through the MgO layer, and thus there is no central peak at $\mathbf{k}_\parallel = 0$. Instead there are transmission spikes scattered around in the Brillouin zone and these are related to interface states, i.e. **k**-points where there is a large density of states in the central region and therefore an increased probability of tunneling.

The above discussion shows that the majority electrons dominate the conductance for parallel magnetization of the electrodes. To obtain the TMR this conductance must be compared with the conductance for anti-parallel magnetization of the electrodes. In this case a majority state of one electrode is coupling with the minority state of the other electrode. Due to the different symmetries of the minority and majority bands, the conductance at $\mathbf{k}_\parallel = 0$ will be strongly suppressed and the conductance thereby much smaller than for the parallel case. The result of such a calculation is reported in [22], and the calculated TMR values for a number of different interface structures are summarized in table 2.

**Table 2.** The table summarizes the TMR calculated using (12) and area normalized resistance, $RA$, of the Fe–MgO–Fe system with different interface layers between the left Fe electrode and the five MgO layers [22].

| Structure | TMR (%) | $RA$ ($\Omega\ \mu m^2$) |
|---|---|---|
| Fe–MgO–Fe | 2302 | 21 |
| Fe–FeOMgO–Fe | 90 | 317 |
| Fe–AuMgOAu–Fe | 1232 | 5 |
| Fe–NiOMgO–Fe | 58 | 171 |
| Fe–MnOMgO–Fe | 903 | 735 |

For the ideal Fe–MgO–Fe system the calculated TMR value is 2302%. This is one order of magnitude higher than measured experimentally [26]. A very likely origin of this discrepancy is that the idealized theoretical structure is not realized experimentally. In particular, the interface structure between the Fe electrode and the MgO interface plays an important role. Upon growth of the MgO layers on top of the Fe electrode, the deposited O atoms may oxidize the Fe electrode [27]. A simulation of the effect of a single FeO layer between the Fe electrode and the MgO is reported in table 2 and it reveals that such a layer will strongly reduce the TMR value.

A way to avoid the degradation in the TMR due to the oxidation of the Fe electrodes is to put a buffer layer between the electrode and MgO. Simulations of the effect of different buffer layers are shown in table 2 and such simulations may guide experimentalists in their search for the geometries with optimal performance.

## 4. Full semiconductor device simulation

The simulations in the above examples have been limited to rather small systems compared to the scale of CMOS transistors. In order to apply the methodology to full semiconductor device simulations, it must be able to handle many thousand atoms. The extension of the methodology to such large systems is only possible if the computational complexity scales linearly with the system size. In table 1 we list the scaling of the different computational steps in the methodology. We see that except for the Green's function calculation all other parts show nearly linear scaling ($N \log N$ scaling is in practice similar to linear scaling). Thus, for large systems the calculation of the Green's function will be the time limiting part of the simulation.

The so-called recursion formula [28–30] provides an exact approach for calculating the Green's function and this formula scales as $O(NA^3)$ where $N$ is the number of atoms and $A$ the area of the device perpendicular to the transport direction. For a cubic cell we have $A \propto N^{2/3}$ and the overall scaling is $O(N^3)$. However, for long and thin devices the $A^3$ scaling can be neglected, and the Green's function approach allows for exact $O(N)$ electronic structure calculations. A recent variant of the recursion method improves the efficiency when used for calculating the transmission coefficient of the device [31].

It can be shown that the Green's function approach is equivalent to a wavefunction picture where the density is obtained by calculating the eigenstates of the system [32]. The eigenstates of the two-probe systems are most conveniently described using the so-called scattering states. A scattering state has an initial state in one of the electrodes and describes the electron propagation through the device, part of the wave being reflected and another part being transmitted. At a given energy there are only very few propagating states, the remaining states being evanescent waves which quickly die off inside the device. This observation may be exploited for developing new superfast approximate algorithms. A promising step is the development of a new iterative scheme for calculating the self-energy matrix by selecting only propagating states, and this approach is more than one order of magnitude faster than currently used algorithms [20].

## 5. Conclusion

We have presented a quantum mechanical approach based on NEGF-DFT for modeling electron transport in nanoscale systems. The methodology has been used for studying the electron transport in emerging electronic devices and spin-dependent electron transport across interfaces. In order to extend the methodology to full semiconductor device models there is a need for new more efficient algorithms. There is extensive research into such new more efficient and parallel algorithms and the simulation of the electrical properties of systems comprising thousands of atoms seems feasible in the near future. Furthermore, new developments within NEGF which include interaction between the electrons and phonons [13] as well as photons [33] show promise for the NEGF-DFT approach to be the backbone of a new generation of semiconductor device modeling tools.

## Acknowledgments

This work was supported by grant number 2106040017, Parallel Algorithms for Computational NanoScience, under the NABIIT program from the Danish Council for Strategic Research and grant number 26-04-0181 from the research council for production and technology.

## References

[1] *The International Technology Roadmap for Semiconductors (ITRS)* 2006 update www.itrs.net
[2] Brandbyge M, Mozos J L, Ordejon P, Taylor J and Stokbro K 2002 *Phys. Rev.* B **65** 165401
[3] Damle P S, Ghosh A W and Datta S 2001 *Phys. Rev.* B **64** 201
[4] Taylor J, Guo H and Wang J 2001 *Phys. Rev.* B **63** 104R
[5] Lang N D 1995 *Phys. Rev.* B **52** 5335
[6] Hirose K and Tsukada M 1995 *Phys. Rev.* B **51** 5278
[7] Mujica V, Roitberg A E and Ratner M A 2000 *J. Phys. Chem.* **112** 6834
[8] Neatona J B, Khoob K H, Spatarub C D and Louie S G 2005 *Comput. Phys. Commun.* **169** 1
[9] Rocha A R *et al* 2006 *Phys. Rev.* B **73** 85414
[10] Ke S-H, Baranger H U and Yang W 2004 *Phys. Rev.* B **70** 85410
[11] Zhang C *et al* 2004 *Phys. Rev.* B **69** 134406
[12] Soler J M *et al* 2002 *J. Phys.: Condens. Matter* **14** 2745

[13] Paulsson M, Frederiksen T and Brandbyge M 2005 *Phys. Rev.* B **72** 201101
[14] Hohenberg P and Kohn W 1964 *Phys. Rev.* **136** B864
[15] Kohn W and Sham L J 1965 *Phys. Rev.* **140** 1133
[16] Perdew J P and Zunger A 1981 *Phys. Rev.* B **23** 5048
[17] Perdew J P, Burke K and Ernzerhof M 1996 *Phys. Rev. Lett.* **77** 3865
[18] Heyd J, Scuseria G E and Ernzerhof M 2003 *J. Chem. Phys.* **118** 8207
[19] Lopez-Sancho M, Lopez-Sancho J and Rubio J 1984 *J. Phys. F: Met. Phys.* **14** 1205
[20] Sørensen H H B, Hansen P C, Petersen D E, Skelboe S and Stokbro K 2007 submitted
[21] Taylor J, Brandbyge M and Stokbro K 2002 *Phys. Rev. Lett.* **89** 138301
[22] Stilling M and Stokbro K 2007 *Proc. NSTI Nanotech. 2007*
[23] Crljen Z, Grigoriev A, Wendin G and Stokbro K 2005 *Phys. Rev.* B **71** 165316
[24] Danilov A, Kubatkin S, Kafanov S, Hedegård P, Stuhr-Hansen N, Moth-Poulsen K and Bjørnholm T 2007 submitted
[25] Butler W H, Zhang X-G, Schulthess T C and MacLaren J M 2001 *Phys. Rev.* B **63** 054416
[26] Yuasa S, Nagahama T, Fukushima A, Suzuki Y and Ando K 2004 *Nat. Mater.* **3** 868
[27] Zhang X-G *et al* 2003 *Phys. Rev.* B **68** 092402
[28] Svizhenko A, Anantram M P, Govindan T R and Biegel B 2002 *J. Appl. Phys.* **91** 2343
[29] Heine V 1980 *Solid State Physics* vol 35, ed H Ehrenreich, F Seitz and D Turnbull (New York: Academic) p 1
[30] Haydock H 1980 *Solid State Physics* vol 35, ed H Ehrenreich, F Seitz and D Turnbull (New York: Academic) p 215
[31] Petersen D E, Sørensen H H B, Hansen P C, Skelboe S and Stokbro K 2007 submitted
[32] Khomyakov P A and Brocks G 2004 *Phys. Rev.* B **70** 195402
[33] Stewart D A and Leonard F 2004 *Phys. Rev. Lett.* **93** 107401